




Article

Thermo-Optical and Particle Number Size Distribution Characteristics of Smoldering Smoke from Biomass Burning

Feng Wang^{1,2} , Qixing Zhang^{1,*} , Xuezhe Xu^{3,4}, Weixiong Zhao³ , Yongming Zhang^{1,*} and Weijun Zhang^{3,4,5}

¹ State Key Laboratory of Fire Science, University of Science and Technology of China, Hefei 230026, China; wfengb@mail.ustc.edu.cn

² School of Environmental Science and Engineering, Yancheng Institute of Technology, Yancheng 224003, China

³ Laboratory of Atmospheric Physico-Chemistry, Anhui Institute of Optics and Fine Mechanics, Chinese Academy of Sciences, Hefei 230031, China; ad09xxz@126.com (X.X.); wxzhao@aiofm.ac.cn (W.Z.); wjzhang@aiofm.ac.cn (W.Z.)

⁴ Graduate School, University of Science and Technology of China, Hefei 230026, China

⁵ School of Environmental Science and Optoelectronic Technology, University of Science and Technology of China, Hefei 230026, China

* Correspondence: qixing@ustc.edu.cn (Q.Z.); zhangym@ustc.edu.cn (Y.Z.); Tel.: +86-551-6360-6457 (Y.Z.)

Received: 29 October 2019; Accepted: 29 November 2019; Published: 3 December 2019



Abstract: Controlled laboratory combustion experiments were conducted in the fire test room to mimic freshly emitted smoldering smoke of biomass burning in China. The biomass components were determined by ultimate analysis and proximate analysis before experiments. The particle number size distribution (PNSD) between 5 and 1000 nm of smoke was measured by a high sampling frequency size spectrometer. A cavity-enhanced aerosol albedometer with wavelength of 532 nm was used to measure scattering coefficients, extinction coefficients, and single scattering albedo (SSA) of smoldering smoke. The PNSDs of smoldering smoke from the burning of agricultural straw could be fitted with a bimodal lognormal distribution as modes around 10 nm (nucleation mode) and 60 nm (Aitken mode). The PNSDs of wood sawdust could be fitted with a trimodal lognormal distribution, while the two modes were in nucleation mode, and one was in Aitken mode. The bulk optical properties (scattering and extinction coefficients) of smoldering smoke had strong correlations with particle number concentrations of sizes bigger than 100 nm. The correlation between SSA and fixed carbon (FC) was strong (the correlation coefficient is 0.89), while the correlation between SSA and volatile matter (VM) or ash was weak. The relationship between SSA and N (or S) showed a positive correlation, while that of SSA and C showed a negative correlation. The relationship between SSA and VM/FC (or N) showed a strong linear relationship ($r^2 > 0.8$). This paper could improve understanding of the relationship between the optical and particle size distribution properties of smoke from biomass burning and the components of biomass materials under similar combustion conditions.

Keywords: single scattering albedo; lognormal distribution; smoldering biomass combustion; fire test room; carbonaceous aerosol

1. Introduction

Different kinds of atmospheric aerosols have different influences on climate [1,2], air quality [3], and human health [4]. One of the most important components of atmospheric aerosols is carbonaceous aerosols, which are comprised of organic and elemental carbon [5,6]. The emissions from biomass

burning are important constituents of global carbonaceous aerosols [7–9]. Approximately 88% of total carbonaceous aerosol mass is emitted from biomass burning, while approximately 80% is emitted from the smoldering combustion phase [10,11]. Particles suspended in the atmosphere can both scatter and absorb solar radiation and terrestrial radiation [12]. The optical and physical properties of atmospheric aerosols from biomass burning should be investigated.

However, large uncertainties exist in the measurement of light absorption of carbonaceous aerosols from both laboratory experiments and field observations [13] for the complexity of biomass burning. Experiments were conducted in the combustion facility of the United States Department of Agriculture (USDA) Forest Service Fire Sciences Laboratory (FSL) as part of a comprehensive study to investigate the complicated physical, optical, and chemical properties of smoke particles emitted from combustion of common mid-latitude wildland fuels in the United States [14–16]. They found that smoldering combustion emissions favored larger sizes (about 100 nm) and a unimodal distribution within 3 h after emission, while light scattering dominated light extinction with a single scattering albedo greater than 0.95 [15]. Number size distributions of tar ball from the smoldering of wildland fuels observed in scanning electron microscopy images showed major peaks at large diameters (around 500 nm) and the other peaks at small diameters (around 130 nm), in contrast to previous observations of tar balls from biomass fires [16]. The direct observation of spherical carbonaceous particles with size distributions of a single peak at about 70 nm in diameter was acquired from a smoldering combustion of two commonly dry mid-latitude fuels on a flat fuel bed which produced white smoke that filled a large chamber [11]. Janhäll et al. [17] explored and characterized the variability of the particle size distribution of fresh smoke from different vegetation fires, which was typically dominated by a lognormal accumulation mode with count a median diameter of around 120 nm, depending on age, fuel, and combustion efficiency. Similar to for biomass burning, aerosols from various coal combustion show different physicochemical characteristics for their various inherent properties and different combustion conditions [18–20]. Pintér et al. [21] have provided the optical properties of carbonaceous aerosols generated from various coal combustion and their correlations with the thermochemical and energetic properties of the coal samples. There could be a strong linear correlation between the calorific value of the investigated coal bulk materials and single scattering albedo of carbonaceous particulate matter generated from them. These early studies provide useful but insufficient information for smoke from various biomass burning, which have different properties depending on fuel and combustion conditions [22]. Most of these experiments were conducted in the laboratory with large differences for field measurements. However, even if field measurements represent real world burning more than laboratory experiment, the results were influenced by different kinds of conditions with complex reasons for occurring [23].

In this paper, the components of biomass samples in China were determined by the ultimate analysis and proximate analysis. The controlled laboratory combustion experiments were conducted in the fire test room to generate smoldering smoke from biomass burning in a steady combustion condition. Smoke could be diffused and mixed with the air naturally. Measurements included scattering and extinction coefficients as well as the particle number size distribution (PNSD). This paper aimed to investigate the relationship between the optical and particle size distribution properties of smoldering smoke as well as the components of biomass materials under similar combustion conditions.

2. Materials and Methods

2.1. Materials

In this study, all biomass samples were obtained from a variety of sources in China as a reference point. Four kinds of agricultural straw were selected in Shou County of Anhui Province, namely soya, wheat, corn, and rice. Five kinds of wood sawdust were also prepared for experiments. The kinds of wood sawdust were phoenix tree (as Ph), poplar (as Po), picea (as Pi), and three kinds of pines (as P1, P2, and P3). The ultimate analysis and proximate analysis were carried out to determine the properties

of the biomass samples. All of the biomass samples were grinded, sieved by screen mesh of 300 μm , and dried at a temperature of 105 $^{\circ}\text{C}$ for about 24 h in a drying cabinet before ultimate analysis and proximate analysis.

The ultimate analysis was carried out with Vario EL cube (Elementar) to determine the major elements of biomass samples, including the contents of carbon (C), oxygen (O), hydrogen (H), nitrogen (N), and sulfur (S).

The proximate analysis was carried out to determine the constituents with various states of thermal stability in biomass samples, namely moisture (M), volatile matter (VM), fixed carbon (FC), and ash (A), according to the ASTM standard methods [24–26] in a thermal analyzer (Netzsch STA 449F3) with two steps. The first step was conducted using nitrogen (N_2) with a gas flow rate of 50 mL/min. The sample was heated from room temperature to 110 $^{\circ}\text{C}$ with a heating rate of 30 $^{\circ}\text{C}/\text{min}$, and followed by a hold time of 10 min for isothermal condition of 110 $^{\circ}\text{C}$ to determine the mass of M. VM was released when the sample was heated up to 950 $^{\circ}\text{C}$ and cooled down to 450 $^{\circ}\text{C}$ with a temperature rate of 30 $^{\circ}\text{C}/\text{min}$. Following that, the flow gas was changed to air with a gas flow rate of 50 mL/min. The sample was burnt out from 450 $^{\circ}\text{C}$ to 800 $^{\circ}\text{C}$ with a temperature rate of 30 $^{\circ}\text{C}/\text{min}$ in this step. The ash content was received as the final residue. The mass of FC was calculated according to the mass of VM and ash. The proximate analysis of VM, FC, and ash was conducted to determine dryness, therefore the constituents of VM, FM, and ash have the relationship as follows,

$$V + F + A = 100\%, \quad (1)$$

in which V , F , and A are the mass ratios of VM, FC, and ash contents to the total mass of biomass samples on the dry basis of proximate analysis. All the experiments of proximate analysis were repeated three times.

2.2. Experimental Methods

Experiments were conducted in a fire test room with a size of 10 m in length, 7 m in width and 4 m in height. The fire test room is located in State Key Laboratory of Fire Science at the University of Science and Technology of China [27]. The room was used to mimic smoldering biomass combustion scenarios in the field by using measurements with appropriate dilution of the combustion emissions and fuel arrangements to approximate and steady combustion conditions, similar to for chamber experiments of biomass burning [28–30]. The fire test room was sealed during combustion and sampling with the exhaust closed. After the biomass samples were burnt out, the smoke from the whole smoldering fire was well mixed with air in the room, sampled at the corner of 1.92 m height, and distributed through a manifold to a high sampling frequency size spectrometer (flow rate of 7.5 L/min; DMS500, Cambustion Ltd., Cambridge, UK) and a cavity-enhanced aerosol albedometer with wavelength of 532 nm (flow rate of 1.3 L/min; Anhui Institute of Optics and Fine Mechanics, Hefei, China). The sample flow rate was 4.4 L/min. The dilution gas was N_2 with a flow rate of 4.4 L/min. The PNSD between 5 and 1000 nm was measured every 3 s with DMS500 [31,32] and the calibration of DMS was derived from spherical particles with the inversion matrix of unconstrained lognormal parameterization. The cavity-enhanced aerosol single-scattering albedometer was based on a light-emitting-diode (LED) incoherent broadband cavity-enhanced absorption spectroscopy (IBBCEAS) system combined with an integrating sphere (IS) for simultaneous in situ measurements of aerosol extinction and scattering coefficients in an exact same sample volume [33–35]. The detection limits for the scattering and extinction channels with 9 s integration time were 0.54 and 0.15 Mm^{-1} , respectively. The aerosol light absorption can be quantitatively expressed using single scattering albedo (SSA) which is defined by the ratio of aerosol light scattering to aerosol light extinction (the sum of absorption and scattering). For non-absorbing aerosols, SSA is 1. The total uncertainty in the measurements of SSA was estimated to be less than 5% [35]. The experiments of soya, wheat, corn, rice, and Pi were repeated three times. The experiments of Po and Pi were repeated twice. The results showed a good repeatability with a

maximum uncertainty of SSA of less than 4% for Po. A schematic diagram of the fire test room and the experimental setup is shown in Figure 1.

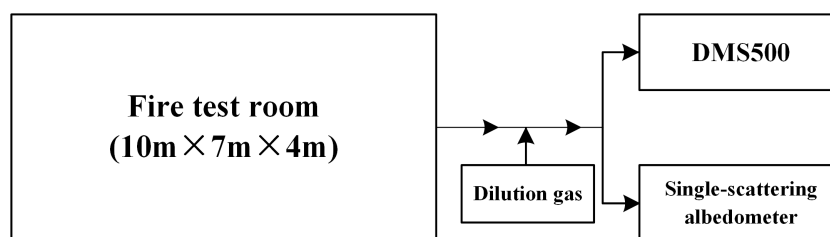


Figure 1. Schematic diagram of the fire test room and the experimental setup.

The biomass samples were put in the room with similar temperature and humidity for more than 24 h before experiments. In the experiments, the samples of agricultural straw were cut to pieces of 4–6 cm in length, and the samples of wood sawdust were sieved by screen mesh of 300 μm . About 5 g of biomass sample was put in a container made of aluminum foil with size of 10 cm \times 10 cm in the center of the room. All the biomass samples were burned on a heater (OMEGALUX) with a size of 30 cm \times 30 cm. The combustion state of biomass samples was controlled at smoldering by the voltage of the heater (about 100 V, with the thermal radiation power of 4.5 kW/m²) in every experiment. Before every experiment, the particle size distribution and optical properties of aerosol in the fire test room were measured for about 5 min as the background data. During every experiment, the door and windows of the room were closed to reduce the influence from outside. After about 10–25 min, the samples burnt out and smoke from the whole smoldering fire was well mixed in the fire test room and monitored under approximately steady-state for up to several minutes. If the optical properties of sampled smoke were approximately steady for more than 5 min, which meant the fluctuations of the scattering and extinction coefficients did not exceed 5% at last, then the experiment was finished. After experiments, the windows and exhaust were opened to clean air in the room. Temperature and relative humidity in the fire test room were recorded for all experiments with the average values of 18.5 $^{\circ}\text{C} \pm 0.6$ $^{\circ}\text{C}$ and 47.8% $\pm 8.0\%$, respectively.

3. Results and Discussion

3.1. Results of Ultimate Analysis and Proximate Analysis

The results of ultimate analysis and proximate analysis are listed in Table 1, as the properties of the biomass samples. As seen in Table 1, the contents of the major elements in agricultural straw and wood are quite different. The contents of C in wood are higher than in agricultural straw. Conversely, the contents of N and S in wood are significantly lower than in agricultural straw. The contents of O in agricultural straw are lower than in wood except for soya and Ph. The contents of C, O, and H in rice straw are lower than other biomass samples. The sum of five major elements are lower than 85% for rice straw, while that of other biomass samples are higher than 90%, especially for wood.

Table 1. The ultimate analysis and proximate analysis of biomass samples.

Biomass Samples	Ultimate Analysis (wt.%)					Proximate Analysis (wt.%)			
	C	O	H	N	S	VM	FC	Ash	M
Soya	41.31	45.61	6.40	0.870	0.319	74.61	19.81	5.58	10.61
Wheat	42.48	43.69	6.21	0.590	0.470	75.61	15.30	9.09	7.51
Corn	41.66	43.86	6.14	0.587	0.342	71.59	20.19	8.21	10.16
Rice	36.72	40.41	5.83	0.527	0.538	66.43	14.89	18.68	8.93
Average	40.54	43.39	6.14	0.644	0.417	72.06	17.55	10.39	9.30
SD¹	2.60	2.17	0.24	0.154	0.104	4.12	2.84	5.72	1.39

Table 1. Cont.

Biomass Samples	Ultimate Analysis (wt.%)					Proximate Analysis (wt.%)			
	C	O	H	N	S	VM	FC	Ash	M
Ph	46.03	42.43	6.01	0.178	0.167	66.64	12.09	21.27	6.01
Po	46.43	45.29	6.10	0.140	0.122	72.89	14.80	12.31	9.42
Pi	47.90	45.29	6.33	0.045	0.048	82.89	14.45	2.66	9.14
P1	46.23	44.10	6.12	0.038	0.052	72.29	11.22	16.49	8.10
P2	46.76	45.17	6.20	0.110	0.105	79.82	15.35	4.83	9.31
P3	47.44	45.73	6.34	0.028	0.031	83.99	13.07	2.94	8.02
Average	46.80	44.67	6.18	0.090	0.088	76.42	13.50	10.08	8.33
SD¹	0.73	1.22	0.13	0.062	0.052	6.87	1.64	7.80	1.29

¹ SD: standard deviation.

The average contents of C, H, and O in agricultural straw are $40.54\% \pm 2.60\%$, $6.14\% \pm 0.24\%$, and $43.39\% \pm 2.17\%$, respectively, while that in wood are $46.80\% \pm 0.73\%$, $6.18\% \pm 0.13\%$, and $44.67\% \pm 1.22\%$, respectively. The average contents of C, H, and O are all higher in wood than in agricultural straw. The contents of C, H, and O in wood are in a narrow range. The results of agricultural straw are also similar except for rice straw. The Van Krevelen diagram in Figure 2 shows the elemental compositional differences between biomass samples of wood and agricultural straw. The ultimate analysis results of biomass samples are similar to the results of other researchers [36–38].

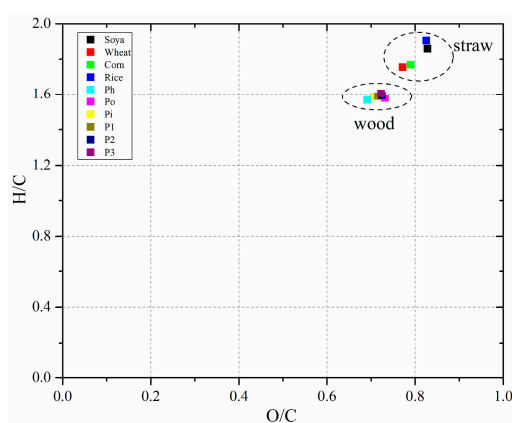


Figure 2. Van Krevelen diagram of biomass samples with the atom ratios of H/C and O/C from the ultimate analysis results.

Different kinds of biomass have different contents of VM, FC, and ash [25,26,36,37]. Pi has the highest content of VM but the lowest content of ash. The contents of VM in rice straw and Ph are lower than the other biomass samples, while the contents of ash are higher than the other biomass except for Ph. The corn straw has the highest content of FC, while P1 has the lowest. The average contents of VM, FC, and ash in agricultural straw are $72.06\% \pm 4.12\%$, $17.55\% \pm 2.84\%$, and $10.39\% \pm 5.72\%$, respectively, while that in wood are $76.42\% \pm 6.87\%$, $13.50\% \pm 1.64\%$, and $10.08\% \pm 7.80\%$, respectively. The average contents of FC and ash are lower in wood than in agricultural straw, while that of VM is higher in wood than in agricultural straw. The content distributions of VM, FC, and ash are dispersed in the large range. The contents of FC in biomass samples are mainly in the range of 10–20%. The contents of VM and ash are in the range of 60–85% and 0–20%, respectively. The contents of VM and ash in biomass samples are in the relationship of a negative correlation ($r^2 = 0.81$), and the Pearson's correlation coefficient (PCC) is -0.89103 , as shown in Figure 3. The char and alkali metals possessed a catalytic effect on the thermal degradation of biomass during pyrolysis [39], with ash of abundant alkaline elements produced [40]. The total liquid and organic yields (representation of VM) increase, while ash composition decrease.

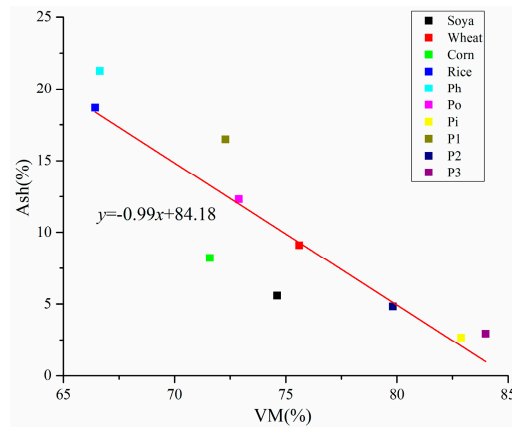


Figure 3. Correlation between the contents of volatile matter (VM) and ash from the proximate analysis results of biomass samples on dry basis.

3.2. Particle Number Size Distribution (PNSD)

The normalized PNSD of smoke particle could be best fitted with lognormal functions [27]:

$$\frac{dN}{dD} = \sum_n \frac{1}{\sqrt{2\pi} D \ln \sigma_g} \exp \left[-\frac{1}{2} \left(\frac{\ln D - \ln D_g}{\ln \sigma_g} \right)^2 \right], \quad (2)$$

in which N is the total number concentration of particles per volume, D is size diameter of particles, D_g is geometry mean diameter (GMD) of particles, σ_g is geometric standard deviation (GSD), and n stands for the number of modes. If $n = 1$, it means there is a unimodal lognormal distribution; it is a bimodal lognormal distribution when $n = 2$; $n = 3$ means a trimodal lognormal distribution; and so on.

The PNSDs of aerosols are influenced by short fluctuations in different kinds of emission sources [41], which can be a part of data set in source apportionment of aerosol particles. In the PNSDs, two modes were identified with D_g about 20 nm and 100 nm from transit traffic and household heating, respectively [42,43]. As a major source of fine particles in the atmosphere, the size distributions of freshly emitted smoke particles from biomass burning resided mainly within the accumulation mode, with D_g at 50–200 nm [2]. The discrepancy of D_g and distribution pattern related to fuel type, combustion environment and conditions, and the aging process [44]. For different kinds of biomass samples, the PNSDs of smoke from smoldering burning were quite different with each other and from results from other researchers [15,45–49]. As shown in Figure 4, the PNSD of soya has two modes, which can be fitted with a bimodal lognormal distribution. Meanwhile, the PNSD of P2 can be fitted with a trimodal lognormal distribution, which has three modes.

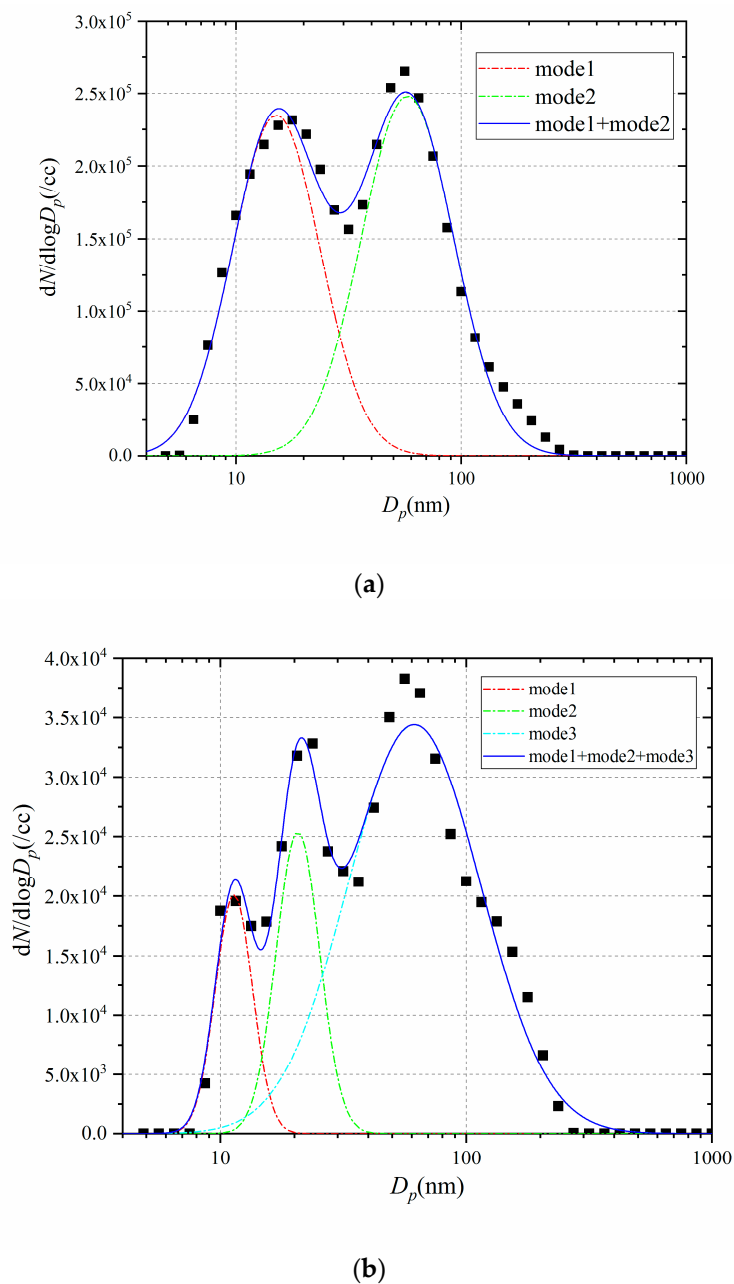


Figure 4. Two kinds of particle size distributions and their fitted curves in the well-mixed stage after burning out. **(a)** Particle size distribution of soya which has two modes; **(b)** particle size distribution of P2 which has three modes.

The PNSDs of aerosol from biomass burning can be fitted with bimodal or trimodal lognormal functions [30,50]. The PNSDs of smoke from smoldering burning of agricultural straw are similar and can be fitted with a bimodal lognormal distribution, with the average values of mode size are $12.71 \text{ nm} \pm 0.71 \text{ nm}$ and $58.42 \text{ nm} \pm 8.64 \text{ nm}$, respectively. The PNSD of wood sawdust can be fitted with a trimodal lognormal distribution, with the average values of mode size at $10.25 \text{ nm} \pm 2.18 \text{ nm}$, $19.81 \text{ nm} \pm 5.50 \text{ nm}$, and $66.70 \text{ nm} \pm 11.18 \text{ nm}$, respectively. The fit parameters of multimodal lognormal distribution are shown in Table 2. The majority of particles by number are mainly in the nucleation ($D_p < 30 \text{ nm}$) and Aitken modes ($30 \text{ nm} < D_p < 100 \text{ nm}$) [49]. The two modes of agricultural straw are around 10 nm (nucleation mode) and 60 nm (Aitken mode). The two modes of wood sawdust are in nucleation mode, and one is in Aitken mode. The D_g of mode 1 for Ph and Po are similar, while that of mode 2 for Ph, Pi, P1, and P2 are similar. However, the D_g of mode 2 for Po is similar to that of

mode 1 for Pi, P1, and P2. The characteristic modes are similar to the characteristics of particle size distributions in lab scale biomass fires of southwestern United States fuels [47] in which the major modes of PNSD of smoldering smoke ranged from 10 nm to 40 nm, but the PNSDs were slightly different because they showed bimodal distributions. During the biomass burning events [44,51], the PNSDs of aerosol showed trimodal distributions, with nucleation ($D_g = 16$ nm or 9.0 nm), Aitken ($D_g = 52$ nm or 31.0 nm), and accumulation ($D_g = 130$ nm or 102 nm). The results were similar to our results in the nucleation and Aitken modes, except for the accumulation modes. The accumulation mode with a larger particle size could be aged particles after a long-range transport, while the smaller particles in the nucleation and Aitken modes were freshly emitted near the sources of biomass burning [44].

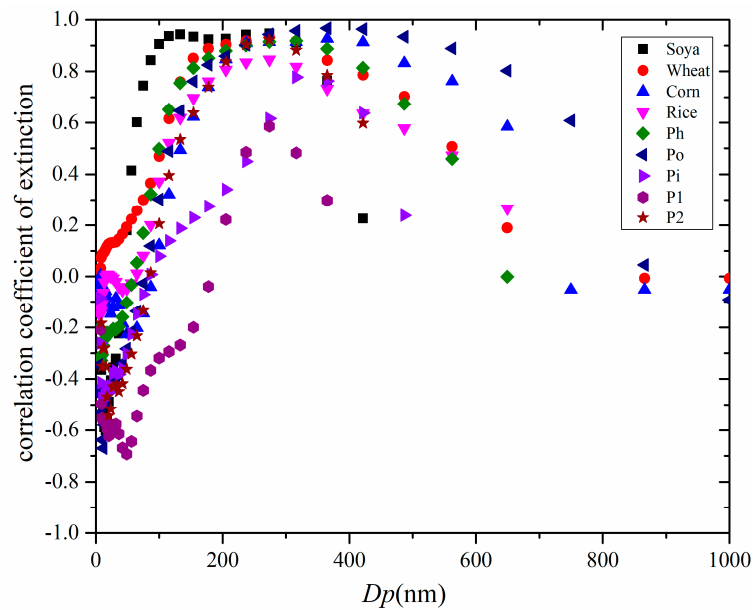
Table 2. Lognormal fit parameters of particle number size distribution for smoldering smoke from biomass burning.

Biomass Samples	Mode 1		Mode 2		Mode 3	
	D_g (nm)	σ_g	D_g (nm)	σ_g	D_g (nm)	σ_g
Soya	12.17	1.391	68.61	1.565	/	/
Wheat	13.74	1.398	51.28	1.622	/	/
Corn	12.30	1.376	62.58	1.811	/	/
Rice	12.63	1.416	51.22	1.535	/	/
Average	12.71	1.395	58.42	1.633	/	/
SD	0.71	0.017	8.64	0.124	/	/
Ph	7.93	1.185	20.26	1.558	56.21	1.679
Po	7.32	1.150	12.29	1.310	66.52	1.804
Pi	10.71	1.193	20.16	1.280	87.99	1.630
P1	12.98	1.271	28.93	1.459	67.18	1.229
P2	11.35	1.164	20.65	1.194	61.50	1.721
P3	11.20	1.169	16.59	1.284	60.83	2.282
Average	10.25	1.189	19.81	1.348	66.70	1.724
SD	2.18	0.043	5.50	0.134	11.18	0.339

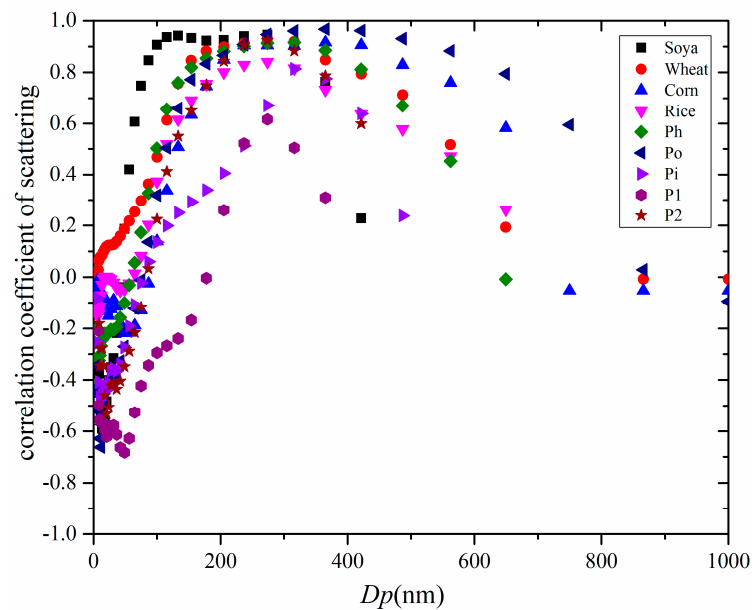
3.3. Correlations between Bulk Optical Properties and PNSDs

The scattering and extinction coefficients (Mm^{-1}) would be changed with particle number concentrations of smoke. SSA is near 1 for smoldering smoke, which means light scattering is much stronger than light absorption. Therefore, the bulk optical properties of smoldering smoke are also related to the particle sizes for different kinds of smoke [21,52]. To set up the relationship between optical properties and PNSDs, the PCCs of bulk optical properties (extinction and scattering coefficients) and particle number concentrations of different sizes were analyzed. We show the correlation coefficients between extinction coefficients/scattering coefficients and particle number concentrations of different sizes for smoldering smoke from biomass burning in Figure 5. For soya, the extinction coefficient has strong correlations with particle number concentrations of sizes from 87 nm to 316 nm ($PCC > 0.8$). The size ranges of strong correlation are from 154 nm to 365 nm for wheat ($PCC > 0.8$), from 205 nm to 487 nm for corn ($PCC > 0.8$), and from 205 nm to 316 nm for rice ($PCC > 0.8$), respectively. The size ranges of strong correlation are changed from 154 nm to 422 nm for Ph ($PCC > 0.8$), from 178 nm to 649 nm for Po ($PCC > 0.8$), and from 205 nm to 316 nm for P2 ($PCC > 0.8$), respectively. The extinction coefficient has relative strong correlations with particle number concentrations of sizes from 274 nm to 422 nm for Pi ($PCC > 0.6$), and from 237 nm to 365 nm for P1 ($PCC > 0.5$). The scattering and extinction coefficients showed similar trends for smoldering smoke. Therefore, the correlation of the scattering coefficient and particle number concentrations of different sizes is similar to that of the extinction coefficient. The flow rate of DMS was changed in the measurements of smoldering smoke of P3, and the relationship between extinction coefficients/scattering coefficients and particle number concentrations was not matched, so the results of P3 are not displayed in Figure 5. As a conclusion, the bulk optical properties

of smoldering smoke have strong correlations with particle number concentrations of sizes bigger than 100 nm.



(a)



(b)

Figure 5. The correlation coefficients between extinction coefficients (a) scattering coefficients (b) and particle number concentrations of different sizes for smoke of biomass samples.

3.4. Correlations between SSA and Contents of Ultimate Analysis and Proximate Analysis

After the sample was burned out, the aerosol in the room mixed sufficiently and became approximately steady as the fresh smoke emitted in the field measurements. We picked the averaged values of last 5 min as the characteristics of a well-mixed stage. SSA of smoldering smoke from burning of biomass samples is similar to the result of smoldering smoke from biomass burning [53–55]. Pintér et al. [21] have given the correlations between inherent optical properties of carbonaceous

aerosols generated from various coals and the thermochemical or energetic properties of the bulk coal samples. The smoldering combustion of biomass consists of two fundamental stages [56,57]. Tar (also as VM) is released from biomass in the first stage. Following that, the remaining char (FC) is burned in the second stage. The two stages could take place simultaneously or subsequently. There could be a correlation relationship between the optical properties of smoke generated from smoldering combustion and the inherent thermochemical properties of biomass samples. Table 3. reveals the correlation coefficients between SSA and the contents of ultimate analysis and proximate analysis of biomass samples, including elements (C, N, and S), and thermochemical properties (FC, VM/FC). It is obvious that the correlations between SSA and VM/FC (or FC, C, N and S) are significantly strong at the significance level of 0.05. The relationship between SSA and N, S, or FC shows a positive correlation, while that of SSA and VM/FC or C shows a negative correlation. However, the correlation between SSA and volatile (or ash) is weak, which is not displayed in the table.

Table 3. The correlation coefficients of single scattering albedo (SSA) and the contents of ultimate analysis and proximate analysis.

Contents	Correlation Coefficient
C	−0.71042
N	0.89636
S	0.72526
FC	0.88980
VM/FC	−0.93748

We found a strong linear correlation between SSA and VM/FC (or N) ($r^2 = 0.88$ for VM/FC and 0.80 for N), as seen in Figure 6. It can be viewed as follows,

$$SSA = -0.04VM/FC + 1.087, \tag{3}$$

$$SSA = 0.12473N + 0.84431, \tag{4}$$

in which VM is the fraction of volatile matter in mass (wt.%), FC is the fraction of fixed carbon in mass (wt.%), and N is the fraction of element N in mass (wt.%).

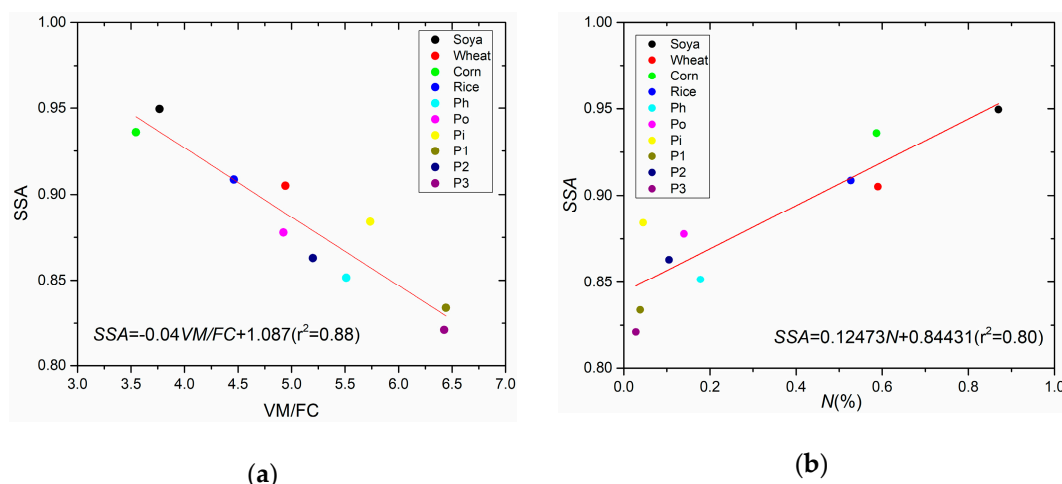


Figure 6. Correlation between SSA and the biomass components: (a) VM/FC; (b) N.

4. Conclusions

Controlled laboratory combustion experiments were conducted in a fire test room to mimic freshly emitted smoldering smoke of biomass burning and the relevant field measurements from China. The PNSDs between 5 and 1000 nm, aerosol scattering coefficients, extinction coefficients, and SSA

were measured. The constituents of biomass samples were determined by the ultimate analysis and proximate analysis.

The contents of the major elements in agricultural straw and wood were quite different. The average contents of C, H, and O were all higher in wood than in agricultural straw. The content distributions of C, H, and O were narrower in wood than in agricultural straw. Meanwhile, the contents of N and S in wood were significantly lower than in agricultural straw. The average contents of FC and ash were lower in wood than in agricultural straw, while that of VM was higher in wood than in agricultural straw. The content distributions of VM, FC, and ash were dispersed in a large range.

We also revealed the PNSD characteristics of smoldering smoke from biomass burning. For different kinds of biomass samples, the PNSDs of smoldering smoke were quite different from each other. The PNSDs of smoldering smoke from burning of agricultural straw could be fitted with a bimodal lognormal distribution as modes of around 10 nm (nucleation mode) and 60 nm (Aitken mode). The PNSDs of wood sawdust could be fitted with a trimodal lognormal distribution, while the two modes were in nucleation mode, and one was in Aitken mode.

We found the correlations between the bulk optical properties (scattering, extinction coefficients, or SSA) and particle sizes of smoldering smoke or the biomass components. The bulk optical properties (scattering and extinction coefficients) of smoldering smoke had strong correlations with particle number concentrations of sizes bigger than 100 nm. The correlation between SSA and FC was strong, while the correlation between SSA and VM (or ash) was weak. The relationship between SSA and N (or S) showed a positive correlation, while that of SSA and C showed a negative correlation. The relationship between SSA and VM/FC (or N) showed a strong linear correlation ($r^2 > 0.8$). However, the small number of biomass samples and combustion conditions limit the universality of conclusions to be drawn. Further experiments of different biomass samples and combustion conditions should be conducted to demonstrate and quantify the thermochemical, optical, and particle size distribution properties, and their relations to each other of aerosols from various biomass burning.

This study could improve the understanding of the relationship between physical properties of smoke and the components of biomass materials under the similar combustion conditions. It would help us to better understand the characteristics of particles from real-world combustion scenarios as well as their impacts on indoor air quality and regional atmospheric environments.

Author Contributions: Conceptualization, F.W., and X.X.; methodology, Q.Z. and W.Z. (Weixiong Zhao); resources, Y.Z. and W.Z. (Weijun Zhang); investigation, F.W. and X.X.; writing—Original draft preparation, F.W.; writing—Review and editing, Q.Z., X.X. and W.Z. (Weixiong Zhao); funding acquisition, Q.Z., W.Z. (Weixiong Zhao), Y.Z. and W.Z. (Weijun Zhang).

Funding: This research was funded by the National Natural Science Foundation of China (Grant No. 41675024, 41330424, and U1733126), the Natural Science Foundation of Anhui Province (Grant No. 1508085J03), the Youth Innovation Promotion Association CAS (Grant No. 2016383), and Fundamental Research Funds for the Central Universities (Grant No. WK2320000040).

Conflicts of Interest: The authors declare no conflict of interest.

References

1. Boucher, O. *Atmospheric Aerosols: Properties and Climate Impacts*; Springer: Dordrecht, The Netherlands, 2015. [[CrossRef](#)]
2. Chen, J.M.; Li, C.L.; Ristovski, Z.; Milic, A.; Gu, Y.T.; Islam, M.S.; Wang, S.X.; Hao, J.M.; Zhang, H.F.; He, C.R.; et al. A review of biomass burning: Emissions and impacts on air quality, health and climate in China. *Sci. Total Environ.* **2017**, *579*, 1000–1034. [[CrossRef](#)] [[PubMed](#)]
3. Pinter, M.; Utry, N.; Ajtai, T.; Kiss-Albert, G.; Jancsek-Turoczi, B.; Imre, K.; Palagyi, A.; Manczinger, L.; Vagvolgyi, C.; Horvath, E.; et al. Optical properties, chemical composition and the toxicological potential of urban particulate matter. *Aerosol. Air Qual. Res.* **2017**, *17*, 1515–1526. [[CrossRef](#)]
4. Anderson, J.O.; Thundiyil, J.G.; Stolbach, A. Clearing the air: A review of the effects of particulate matter air pollution on human health. *J. Med. Toxicol.* **2012**, *8*, 166–175. [[CrossRef](#)] [[PubMed](#)]

5. Katrinak, K.A.; Rez, P.; Buseck, P.R. Structural variations in individual carbonaceous particles from an urban aerosol. *Environ. Sci. Technol.* **1992**, *26*, 1967–1976. [[CrossRef](#)]
6. Grieshop, A.P.; Logue, J.M.; Donahue, N.M.; Robinson, A.L. Laboratory investigation of photochemical oxidation of organic aerosol from wood fires 1: Measurement and simulation of organic aerosol evolution. *Atmos. Chem. Phys.* **2009**, *9*, 1263–1277. [[CrossRef](#)]
7. Lack, D.A.; Richardson, M.S.; Law, D.; Langridge, J.M.; Cappa, C.D.; McLaughlin, R.J.; Murphy, D.M. Aircraft instrument for comprehensive characterization of aerosol optical properties, part 2: Black and brown carbon absorption and absorption enhancement measured with photo acoustic spectroscopy. *Aerosol. Sci. Technol.* **2012**, *46*, 555–568. [[CrossRef](#)]
8. Martinsson, J.; Azeem, H.A.; Sporre, M.K.; Bergstrom, R.; Ahlberg, E.; Ostrom, E.; Kristensson, A.; Swietlicki, E.; Stenstrom, K.E. Carbonaceous aerosol source apportionment using the Aethalometer model—Evaluation by radiocarbon and levoglucosan analysis at a rural background site in southern Sweden. *Atmos. Chem. Phys.* **2017**, *17*, 4265–4281. [[CrossRef](#)]
9. Andreae, M.O. Emission of trace gases and aerosols from biomass burning—An updated assessment. *Atmos. Chem. Phys.* **2019**, *19*, 8523–8546. [[CrossRef](#)]
10. Einfeld, W.; Ward, D.E.; Hardy, C. Effects of fire behavior on prescribed fire smoke characteristics: A case study. In *Global Biomass Burning: Atmospheric, Climatic, and Biospheric Implications*; MIT Press: Cambridge, MA, USA, 1991; pp. 412–419.
11. Chakrabarty, R.K.; Moosmuller, H.; Chen, L.W.A.; Lewis, K.; Arnott, W.P.; Mazzoleni, C.; Dubey, M.K.; Wold, C.E.; Hao, W.M.; Kreidenweis, S.M. Brown carbon in tar balls from smoldering biomass combustion. *Atmos. Chem. Phys.* **2010**, *10*, 6363–6370. [[CrossRef](#)]
12. Alexander, J.M. Optical Properties of Mineral Dust Aerosol Including Analysis of Particle Size, Composition, and Shape Effects, and the Impact of Physical and Chemical Processing. Ph.D. Thesis, University of Iowa, Iowa City, IA, USA, 2015.
13. Chu, J.E.; Ha, K.J. Quantifying organic aerosol single scattering albedo over the tropical biomass burning regions. *Atmos. Environ.* **2016**, *147*, 67–78. [[CrossRef](#)]
14. McMeeking, G.R.; Kreidenweis, S.M.; Baker, S.; Carrico, C.M.; Chow, J.C.; Collett, J.L.; Hao, W.M.; Holden, A.S.; Kirchstetter, T.W.; Malm, W.C.; et al. Emissions of trace gases and aerosols during the open combustion of biomass in the laboratory. *J. Geophys. Res. Atmos.* **2009**, *114*. [[CrossRef](#)]
15. Carrico, C.M.; Prenni, A.J.; Kreidenweis, S.M.; Levin, E.J.T.; McCluskey, C.S.; DeMott, P.J.; McMeeking, G.R.; Nakao, S.; Stockwell, C.; Yokelson, R.J. Rapidly evolving ultrafine and fine mode biomass smoke physical properties: Comparing laboratory and field results. *J. Geophys. Res. Atmos.* **2016**, *121*, 5750–5768. [[CrossRef](#)]
16. Chakrabarty, R.K.; Moosmüller, H.; Garro, M.A.; Arnott, W.P.; Walker, J.; Susott, R.A.; Babbitt, R.E.; Wold, C.E.; Lincoln, E.N.; Hao, W.M. Emissions from the laboratory combustion of wildland fuels: Particle morphology and size. *J. Geophys. Res. Atmos.* **2006**, *111*. [[CrossRef](#)]
17. Janhall, S.; Andreae, M.O.; Poschl, U. Biomass burning aerosol emissions from vegetation fires: Particle number and mass emission factors and size distributions. *Atmos. Chem. Phys.* **2010**, *10*, 1427–1439. [[CrossRef](#)]
18. Dang, J.; Li, C.; Li, J.; Dang, A.; Zhang, Q.; Chen, P.; Kang, S.; Dunn-Rankin, D. Emissions from solid fuel cook stoves in the Himalayan region. *Energies* **2019**, *12*, 1089. [[CrossRef](#)]
19. Tucki, K.; Orynych, O.; Wasiak, A.; Świć, A.; Wichłacz, J. The impact of fuel type on the output parameters of a new biofuel burner. *Energies* **2019**, *12*, 1383. [[CrossRef](#)]
20. Lai, A.; Shan, M.; Deng, M.; Carter, E.; Yang, X.; Baumgartner, J.; Schauer, J. Differences in chemical composition of PM_{2.5} emissions from traditional versus advanced combustion (semi-gasifier) solid fuel stoves. *Chemosphere* **2019**, *233*, 852–861. [[CrossRef](#)]
21. Pinter, M.; Ajtai, T.; Kiss-Albert, G.; Kiss, D.; Utry, N.; Janovszky, P.; Palasti, D.; Smausz, T.; Kohut, A.; Hopp, B.; et al. Thermo-optical properties of residential coals and combustion aerosols. *Atmos. Environ.* **2018**, *178*, 118–128. [[CrossRef](#)]
22. Guo, F.T.; Ju, Y.H.; Wang, G.Y.; Alvarado, E.C.; Yang, X.J.; Ma, Y.F.; Liu, A.Q. Inorganic chemical composition of PM_{2.5} emissions from the combustion of six main tree species in subtropical China. *Atmos. Environ.* **2018**, *189*, 107–115. [[CrossRef](#)]
23. Zhang, H.F.; Wang, S.X.; Hao, J.M.; Wan, L.; Jiang, J.K.; Zhang, M.; Mestl, H.E.S.; Alnes, L.W.H.; Aunan, K.; Mellouki, A.W. Chemical and size characterization of particles emitted from the burning of coal and wood in rural households in Guizhou, China. *Atmos. Environ.* **2012**, *51*, 94–99. [[CrossRef](#)]

24. ASTM International. *Standard Test Methods for Proximate Analysis of Coal and Coke by Macro Thermogravimetric Analysis*; ASTM International: West Conshohocken, PA, USA, 2015. [[CrossRef](#)]
25. Cai, J.M.; He, Y.F.; Yu, X.; Banks, S.W.; Yang, Y.; Zhang, X.G.; Yu, Y.; Liu, R.H.; Bridgwater, A.V. Review of physicochemical properties and analytical characterization of lignocellulosic biomass. *Renew. Sustain. Energy Rev.* **2017**, *76*, 309–322. [[CrossRef](#)]
26. Garcia, R.; Pizarro, C.; Lavin, A.G.; Bueno, J.L. Biomass proximate analysis using thermogravimetry. *Bioresour. Technol.* **2013**, *139*, 1–4. [[CrossRef](#)] [[PubMed](#)]
27. Xie, Q.; Yuan, H.; Song, L.; Zhang, Y. Experimental studies on time-dependent size distributions of smoke particles of standard test fires. *Build. Environ.* **2007**, *42*, 640–646. [[CrossRef](#)]
28. Selimovic, V.; Yokelson, R.J.; Warneke, C.; Roberts, J.M.; de Gouw, J.; Reardon, J.; Griffith, D.W.T. Aerosol optical properties and trace gas emissions by PAX and OP-FTIR for laboratory-simulated western US wildfires during FIREX. *Atmos. Chem. Phys.* **2018**, *18*, 2929–2948. [[CrossRef](#)]
29. Stockwell, C.E.; Yokelson, R.J.; Kreidenweis, S.M.; Robinson, A.L.; DeMott, P.J.; Sullivan, R.C.; Reardon, J.; Ryan, K.C.; Griffith, D.W.T.; Stevens, L. Trace gas emissions from combustion of peat, crop residue, domestic biofuels, grasses, and other fuels: Configuration and Fourier transform infrared (FTIR) component of the fourth Fire Lab at Missoula Experiment (FLAME-4). *Atmos. Chem. Phys.* **2014**, *14*, 9727–9754. [[CrossRef](#)]
30. Popovicheva, O.; Kozlov, V.; Rakhimov, R.; Shmargunov, V.; Kireeva, E.; Persiantseva, N.; Timofeev, M.; Engling, G.; Eleftheriadis, K.; Diapouli, E. Optical-microphysical and physical-chemical characteristics of Siberian biomass burning: Experiments in aerosol chamber. *Atmos. Ocean. Opt.* **2016**, *29*, 492–500. [[CrossRef](#)]
31. Alderman, S.L.; Ingebrethsen, B.J. Characterization of mainstream cigarette smoke particle size distributions from commercial cigarettes using a DMS500 fast particulate spectrometer and smoking cycle simulator. *Aerosol Sci. Technol.* **2011**, *45*, 1409–1421. [[CrossRef](#)]
32. Reavell, K.; Hands, T.; Collings, N. A fast response particulate spectrometer for combustion aerosols. In *SAE Technical Paper 2002-01-2714*; SAE International: Warrendale, PA, USA, 2002.
33. Singh, S.; Fiddler, M.N.; Bililign, S. Measurement of size-dependent single scattering albedo of fresh biomass burning aerosols using the extinction-minus-scattering technique with a combination of cavity ring-down spectroscopy and nephelometry. *Atmos. Chem. Phys.* **2016**, *16*, 13491–13507. [[CrossRef](#)]
34. Xu, X.Z.; Zhao, W.X.; Zhang, Q.L.; Wang, S.; Fang, B.; Chen, W.D.; Venables, D.S.; Wang, X.F.; Pu, W.; Wang, X.; et al. Optical properties of atmospheric fine particles near Beijing during the HOPE-(3)A campaign. *Atmos. Chem. Phys.* **2016**, *16*, 6421–6439. [[CrossRef](#)]
35. Zhao, W.; Xu, X.; Dong, M.; Chen, W.; Gu, X.; Hu, C.; Huang, Y.; Gao, X.; Huang, W.; Zhang, W. Development of a cavity-enhanced aerosol albedometer. *Atmos. Meas. Tech.* **2014**, *7*, 2551–2566. [[CrossRef](#)]
36. Garcia, R.; Pizarro, C.; Lavin, A.G.; Bueno, J.L. Characterization of Spanish biomass wastes for energy use. *Bioresour. Technol.* **2012**, *103*, 249–258. [[CrossRef](#)] [[PubMed](#)]
37. Telmo, C.; Lousada, J.; Moreira, N. Proximate analysis, backwards stepwise regression between gross calorific value, ultimate and chemical analysis of wood. *Bioresour. Technol.* **2010**, *101*, 3808–3815. [[CrossRef](#)] [[PubMed](#)]
38. Vassilev, S.V.; Baxter, D.; Andersen, L.K.; Vassileva, C.G. An overview of the chemical composition of biomass. *Fuel* **2010**, *89*, 913–933. [[CrossRef](#)]
39. Fahmi, R.; Bridgwater, A.V.; Donnison, I.; Yates, N.; Jones, J.M. The effect of lignin and inorganic species in biomass on pyrolysis oil yields, quality and stability. *Fuel* **2008**, *87*, 1230–1240. [[CrossRef](#)]
40. Vassilev, S.V.; Vassileva, C.G.; Song, Y.C.; Li, W.Y.; Feng, J. Ash contents and ash-forming elements of biomass and their significance for solid biofuel combustion. *Fuel* **2017**, *208*, 377–409. [[CrossRef](#)]
41. Wehner, B.; Wiedensohler, A. Long term measurements of submicrometer urban aerosols: Statistical analysis for correlations with meteorological conditions and trace gases. *Atmos. Chem. Phys.* **2003**, *3*, 867–879. [[CrossRef](#)]
42. Ajtai, T.; Utry, N.; Pinter, M.; Major, B.; Bozoki, Z.; Szabo, G. A method for segregating the optical absorption properties and the mass concentration of winter time urban aerosol. *Atmos. Environ.* **2015**, *122*, 313–320. [[CrossRef](#)]
43. Utry, N.; Ajtai, T.; Filep, A.; Pinter, M.; Torok, Z.; Bozoki, Z.; Szabo, G. Correlations between absorption Angstrom exponent (AAE) of wintertime ambient urban aerosol and its physical and chemical properties. *Atmos. Environ.* **2014**, *91*, 52–59. [[CrossRef](#)]

44. Shang, D.J.; Hu, M.; Zheng, J.; Qin, Y.H.; Du, Z.F.; Li, M.R.; Fang, J.Y.; Peng, J.F.; Wu, Y.S.; Lu, S.H.; et al. Particle number size distribution and new particle formation under the influence of biomass burning at a high altitude background site at Mt. Yulong (3410 m), China. *Atmos. Chem. Phys.* **2018**, *18*, 15687–15703. [[CrossRef](#)]
45. Costa, M.A.M.; Carvalho, J.A.; Neto, T.G.S.; Anselmo, E.; Lima, B.A.; Kura, L.T.U.; Santos, J.C. Real-time sampling of particulate matter smaller than 2.5 μm from Amazon forest biomass combustion. *Atmos. Environ.* **2012**, *54*, 480–489. [[CrossRef](#)]
46. Hossain, A.M.M.M.; Park, S.; Kim, J.S.; Park, K. Volatility and mixing states of ultrafine particles from biomass burning. *J. Hazard. Mater.* **2012**, *205*, 189–197. [[CrossRef](#)] [[PubMed](#)]
47. Hosseini, S.; Li, Q.; Cocker, D.; Weise, D.; Miller, A.; Shrivastava, M.; Miller, J.W.; Mahalingam, S.; Princevac, M.; Jung, H. Particle size distributions from laboratory-scale biomass fires using fast response instruments. *Atmos. Chem. Phys.* **2010**, *10*, 8065–8076. [[CrossRef](#)]
48. Okoshi, R.; Rasheed, A.; Reddy, G.C.; McCrowey, C.J.; Curtis, D.B. Size and mass distributions of ground-level sub-micrometer biomass burning aerosol from small wildfires. *Atmos. Environ.* **2014**, *89*, 392–402. [[CrossRef](#)]
49. Vu, T.V.; Delgado-Saborit, J.M.; Harrison, R.M. Review: Particle number size distributions from seven major sources and implications for source apportionment studies. *Atmos. Environ.* **2015**, *122*, 114–132. [[CrossRef](#)]
50. Rissler, J.; Vestin, A.; Swietlicki, E.; Fisch, G.; Zhou, J.; Artaxo, P.; Andreae, M.O. Size distribution and hygroscopic properties of aerosol particles from dry-season biomass burning in Amazonia. *Atmos. Chem. Phys.* **2006**, *6*, 471–491. [[CrossRef](#)]
51. Ulevicius, V.; Bycenkiene, S.; Bozzetti, C.; Vlachou, A.; Plauskaite, K.; Mordas, G.; Dudoitis, V.; Abbaszade, G.; Remeikis, V.; Garbaras, A.; et al. Fossil and non-fossil source contributions to atmospheric carbonaceous aerosols during extreme spring grassland fires in Eastern Europe. *Atmos. Chem. Phys.* **2016**, *16*, 5513–5529. [[CrossRef](#)]
52. Lyamani, H.; Olmo, F.J.; Alados-Arboledas, L. Light scattering and absorption properties of aerosol particles in the urban environment of Granada, Spain. *Atmos. Environ.* **2008**, *42*, 2630–2642. [[CrossRef](#)]
53. Chakrabarty, R.K.; Arnold, I.J.; Francisco, D.M.; Hatchett, B.; Hosseinpour, F.; Loria, M.; Pokharel, A.; Woody, B.M. Black and brown carbon fractal aggregates from combustion of two fuels widely used in Asian rituals. *J. Quant. Spectrosc. Radiat. Transf.* **2013**, *122*, 25–30. [[CrossRef](#)]
54. Liu, S.; Aiken, A.C.; Arata, C.; Dubey, M.K.; Stockwell, C.E.; Yokelson, R.J.; Stone, E.A.; Jayarathne, T.; Robinson, A.L.; DeMott, P.J.; et al. Aerosol single scattering albedo dependence on biomass combustion efficiency: Laboratory and field studies. *Geophys. Res. Lett.* **2014**, *41*, 742–748. [[CrossRef](#)]
55. Pokhrel, R.P.; Wagner, N.L.; Langridge, J.M.; Lack, D.A.; Jayarathne, T.; Stone, E.A.; Stockwell, C.E.; Yokelson, R.J.; Murphy, S.M. Parameterization of single-scattering albedo (SSA) and absorption Angstrom exponent (AAE) with EC/OC for aerosol emissions from biomass burning. *Atmos. Chem. Phys.* **2016**, *16*, 9549–9561. [[CrossRef](#)]
56. Huang, X.; Rein, G. Thermochemical conversion of biomass in smouldering combustion across scales: The roles of heterogeneous kinetics, oxygen and transport phenomena. *Bioresour. Technol.* **2016**, *207*, 409–421. [[CrossRef](#)] [[PubMed](#)]
57. Wang, H.; van Eyk, P.J.; Medwell, P.R.; Birzer, C.H.; Tian, Z.F.; Possell, M. Identification and quantitative analysis of smoldering and flaming combustion of radiata pine. *Energy Fuels* **2016**, *30*, 7666–7677. [[CrossRef](#)]

